Chemical Physics Letters 694 (2018) 29–34

Contents lists available at ScienceDirect

Chemical Physics Letters

journal homepage: www.elsevier.com/locate/cplett

Research paper

Dewetting transition of water confined between atomically rough surfaces: A lattice gas Monte Carlo simulation study

Liyi Bai, Jihye Jang, Zhengqing Zhang, Joonkyung Jang *

Department of Nanoenergy Engineering, Pusan National University, Busan 46241, Republic of Korea

ARTICLE INFO

Article history:
Received 18 November 2017
In final form 16 January 2018

ABSTRACT

Using lattice gas Monte Carlo simulations, we studied the dewetting transition of water confined between a spherical tip and a plate, which is relevant to atomic force microscopy measurements conducted in water. The dewetting transition was investigated by varying the tip-plate distance, tip size, and the pressure of water. With introduction of an atomic scale roughness (1 < nm) in the tip and the plate, the dewetting transition significantly increased in range and yielded an enhanced hydrophobic force between the tip and the plate. This finding is in agreement with the experimental results previously reported by Singh et al.

1. Introduction

A liquid water droplet sandwiched between hydrophobic surfaces spontaneously evaporates when the surfaces are within a certain distance (D_c). This *dewetting transition* occurs due to the confinement of water and gives rise to a strong attractive force between the two hydrophobic surfaces, which is known as the *hydrophobic force*. The hydrophobic force is much stronger and longer in range compared to the van der Waals force. The dewetting transition and the resultant hydrophobic force are manifested in various phenomena, including protein folding [1–3], self-assembly of amphiphilic molecules into micelles and membranes [4,5], and the opening and closing of ionic channels [6,7].

Given its ubiquity and importance, various theoretical and simulation studies have been carried out to understand the dewetting transition [8,9]. Huang et al. [10] have used molecular dynamics simulations to investigate the dewetting transition in ideal α_2D *de novo* protein chains. Zhou and Berne have studied the dewetting transition in the protein folding [11–14] by modelling mellitin tetramers [13]. These theoretical studies assumed ideal geometries of the surfaces such as two plates or two ellipsoids [11]. On the contrary, real surfaces are rough to some extent. In fact, the presence of an atomic or nano-scale roughness on a surface is a rule rather than an exception. However, it is not completely understood how such a small roughness affects the dewetting transition and the resultant hydrophobic force. Interestingly, Singh et al. reported that the hydrophobic force acting between a spherical tip and a plate [15] is greatly enhanced in its range and magnitude in the presence of a microscale (not atomic or nanoscale) surface roughness.

Herein, we theoretically studied the effect of an atomic scale surface roughness on the hydrophobic force between an atomic force microscope (AFM) tip and a plate. Specifically, we performed extensive Monte Carlo (MC) simulations by employing the lattice gas model for water [16–21]. The lattice gas model enabled us to simulate mesoscale tip and plate geometries that were not accessible in a fully atomistic simulation. By systematically varying the pressure and the tip-plate distance, we examined the dewetting transition and the hydrophobic force. Therefore, the effects of surface roughness on the dewetting transition and hydrophobic force have been investigated in this work.

2. Theory and Monte Carlo simulation methods

The present work focuses on the molecular simulation of the dewetting transition of water confined between a spherical tip and a plate (Fig. 1a). We however introduce a simple continuum theory for the dewetting process to present a theoretical background and to compare with the present simulation. Suppose the dewetting gives rise to a cylindrical cavity of radius r and height D between the tip and the plate. Let Ω_V and Ω_L be the grand potentials of the dewetted and wetted systems, respectively. Then, the difference in the grand potentials, $\Delta\Omega$, is given by Eq. (1) [22].

$$\Delta\Omega = \Omega_V - \Omega_L = (\Delta P)V - (\Delta\gamma)A_S + \gamma_{LV}A_{LV} \quad (1)$$

where V is the volume of the cylindrical cavity, A_S is the area of the solid-vapor interface, A_{LV} is the area of the liquid-vapor interface, and ΔP is the difference between the pressure of the liquid (P_L) and vapor pressure (P_V) (both have the same chemical potential

* Corresponding author.
E-mail address: jkjang@pusan.ac.kr (J. Jang).

https://doi.org/10.1016/j.cplett.2018.01.032
0009-2614/

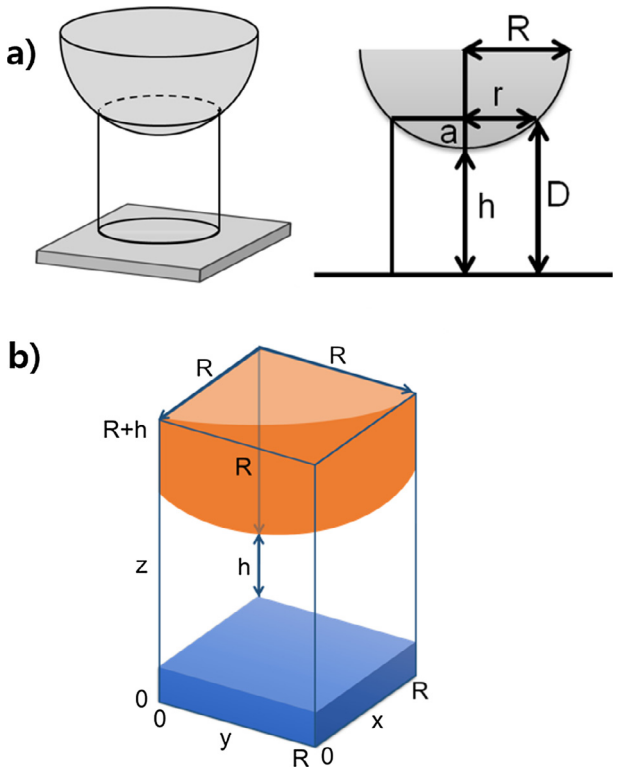

Fig. 1. Geometry of the dewetting transition between a spherical tip (with a radius R) and a plate. (a) Cylindrical cavity assumed in the theory of the dewetting transition. The radius and height of the cylinder are denoted by r and D, respectively. The tip-plate distance is given by h, and $a = D - h$. (b) Simulation cell for the present lattice gas Monte Carlo simulation. Only the first quadrant ($x, y > 0$) is simulated and the rest three quadrants are taken to be mirror images of the first quadrant.

μ). γ_{LV} is the liquid-vapor interfacial tension, and $\Delta\gamma \equiv \gamma_{LS} - \gamma_{VS}$ where γ_{LS} and γ_{VS} are the liquid-solid and vapor-solid interfacial tensions, respectively. By inspection of the geometry, it can be noted that $V = \pi r^2 D - V_{trunc}$, $A_S = A_{trunc} + \pi r^2$, and $A_{LV} = 2\pi rD$, where V_{trunc} and A_{trunc} are the volume and surface area of the tip inside the cylinder, respectively. $V_{trunc} = \pi(Ra^2 - a^3/3)$ and $A_{trunc} = 2\pi Ra$, where $a = D - h$.

By imposing the condition that $\Delta\Omega = 0$, it is possible to solve the equations for the tip-plate distance at the dewetting transition h_c as given in Eq. (2).

$$h_c = \frac{\Delta p(Ra^2 - a^3/3) - \gamma_{LV}\cos\theta(2Ra + r^2)}{\Delta p r^2 + 2\gamma_{LV} r} - a \tag{2}$$

where θ refers to the intrinsic contact angle of a water droplet on a flat surface. The Young equation ($\Delta\gamma = -\gamma_{LV}\cos\theta$) was used to derive Eq. (2). Although Eq. (2) applies to a cylindrical cavity, a real cavity is rather close to an axis symmetric meniscus for which a simple analytical expression such as Eq. (2) cannot be obtained.

The present Monte Carlo simulation is based on the lattice gas model, wherein water molecules reside on the sites of a cubic lattice between a sphere and a plate. A molecule interacts with its nearest neighbor (NN) with an attraction energy ε and has its own chemical potential μ. When it is located adjacent (nearest neighbors) to the surfaces of the tip and plate, it experiences a binding energy of b. The Hamiltonian in the lattice gas model is given by Eq. (3),

$$H = -\varepsilon \sum_{i,j=n,n} c_i c_j - b \sum_{i=surf} c_i - \mu N \tag{3}$$

where c_i is the occupation number at the i^{th} lattice site (0 or 1). In this model, the μ value for the bulk vapor-liquid phase transition, μ_C, is exactly -3ε. The *saturation* of the system is defined as $\exp[(\mu - \mu_C)/(k_B T)]$, which is exact in the ideal gas limit. The bulk critical temperature, T_C, for the lattice gas is given by $1.128\varepsilon/k_B$. In order to emulate a liquid, the saturation was set to 105%. Identifying the liquid as water, ε was set to 4.8 kJ mol^{-1} (because T_C of water is 647.3 K) and the lattice spacing, l, was set to 0.37 nm (molecular diameter of water). The surface binding energy was set to $b = 0.01\varepsilon$, in order to mimic a hydrophobic surface and the temperature was fixed to 300 K.

The present lattice gas model is a standard method to study both gas and liquid phases and the transition between these phases. Numerous previous studies [23–25] on the liquid-gas transitions employed the lattice gas model. This coarse-grained model cannot capture the full molecular features of water such as the dipole moment and the long-ranged Coulomb interaction. However, it has proven to reproduce the essential features of the phase behavior of water. For example, the present lattice gas model was used to successfully simulate the phase transition of water confined in a carbon nanotube [26–28]. Also, the lattice gas simulation reproduced the humidity dependence of the capillary force due to the liquid water formed between an atomic force microscope tip and a surface [22].

The Glauber single spin flip using the Metropolis importance sampling was used for the MC move [29]. Initially, every lattice site was taken to be in the liquid state (by setting its occupancy to 1). In each simulation, 100,000 MC moves were attempted for every lattice site. The initial 60,000 flips were discarded for equilibration and the remaining 40,000 flips were used for calculating the average quantities. We used 5000 configurations to calculate the averages and standard deviations in the densities and cavity widths. A lattice site with an average occupancy larger (less) than 0.5 was considered to be in the liquid (vapor) phase. The density profile, $\rho(x, y, z)$, defined as the average occupancy of the site located at (x, y, z), was also calculated. The width of the cavity was determined from the density profile as follows. For each horizontal position (x, y), we checked vertically the average occupancies of the sites of the column ranging from the lower plate to the upper tip. If all the sites of a column were less than half-full on average, it was declared to be a vapor column. A collection of such vapor columns was cylindrically symmetric around the Z axis. The cavity width was defined as the diameter of this cylinder, and half of this diameter was the radius of the cylindrical cavity r used in Eq. (2). In estimating the cavity width, we also estimated the stability of a cavity. The standard deviation in the diameter relative to its average diameter was defined as the fluctuation of the cavity. A cavity with a fluctuation of more (or less) than 20% was declared as an unstable (or stable) cavity [28]. Only the stable cavities are considered for the calculation of the cavity widths. The unstable cavities are taken to have zero widths.

By varying the tip-plate distance h, we investigated the formation of a stable cavity (with a fluctuation less than 20%). As h decreased to a certain distance h_c, a cavity appeared and broadened with further decreasing h. The cavity width at $h = h_c$ was taken to be the minimum width of the cavity.

The attractive force [24] between the tip and plate separated by h was calculated by Eq. (4),

$$F(h) = -\left(\frac{\partial\Omega}{\partial h}\right)_{\mu,T} - p\left(\frac{\partial V}{\partial h}\right)_{\mu,T} \tag{4}$$

where V is the volume of the cavity, and p is the bulk pressure. The value of Ω was calculated by using the following thermodynamic integration method [30],

$$\beta\Omega = \beta_0\Omega_0 + \int_{\beta_0}^{\beta} H(\beta)d\beta \quad (5)$$

where $\beta = 1/k_BT$ and the subscript zero represents the infinite temperature ($\beta = 0$) at which the grand potential Ω_0 is exactly known. The Ω in Eq. (5) was calculated by running ten independent simulations with different temperatures (β s) followed by numerical integration using the trapezoidal rule [31]. The force, Eq. (4), was then evaluated by taking numerical derivative of Ω with respect to h. The unit of force ε/ℓ is 0.021 nN in the physical dimension.We simulated only the first quadrant of the tip and the plate, and the rest of the quadrants were taken to be mirror images of the first (Fig. 1b). The tip radius was varied as 10, 20, 30, and 40ℓ. The pressure ΔP was varied as 0.08, 1, 8, 25, 50, 75, and 146 atm. It is worth noting that ΔP is related to the saturation by the relation, $\Delta P = \rho_b k_B T \ln$ (saturation), where ρ_b is the bulk number density of the liquid ($=1/\ell^3$). The roughness of the tip or plate was defined as the root-mean-square (RMS) height of each lattice point on the surface measured from a smooth surface (tip or plate). The RMS roughnesses of the tip and plate were 0.4 nm.

The theoretical h_c, determined from Eq. (2), required γ_{LV}, θ, and r values as input. To compare with the lattice gas simulation, we assumed that r was the minimum radius of a stable cavity measured in the present simulation (see above). The parameter γ_{LV} was taken to be half of the work of cohesion, the free energy change where two unit areas of the liquid are separated from the contact [32]. The work of cohesion was approximated as ε/l^2 by neglecting the entropic contribution. On the other hand, γ_{LS} could be written as $\gamma_{LS} = \gamma_{LV} + \gamma_{VS} - W_{LS}$, where W_{LS} is the work of adhesion between the solid and the liquid [33]. Using the approximation $W_{LS} \approx b/l^2$ and the Young equation ($\gamma_{LS} - \gamma_{VS} = -\gamma_{LV}cos\theta$), the value of θ was obtained from the expression $b = (1 + \cos\theta)\varepsilon/2$ [16,34]. The zero temperature approximations for γ_{LV} and W_{LS} have been previously shown to be reasonable [16,24].

All the MC simulations were run by using an in-house Fortran 90 code and by using Xeon 3.0 GHz servers. Using 16 cores of them, a typical Monte Carlo simulation with 100,000 MC moves took 18 CPU hours.

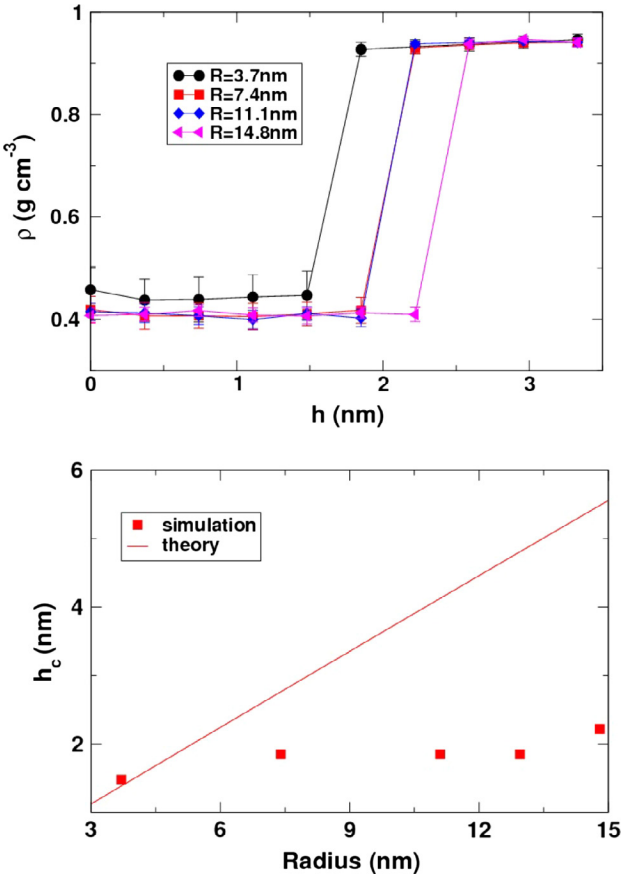

Fig. 2. Effect of the tip size on the dewetting transition. By varying the tip radius R from 3.7 to 14.8 nm, the average density (occupancy) of water was plotted vs. the tip-plate distance h (top). The error bars represent the standard deviations of the densities. Plot of the tip-plate distance at the dewetting transition h_c vs. the tip radius (bottom). The results from the MC simulation and theory are drawn as squares and a solid line, respectively.

3. Results and discussion

Fig. 2 (top) shows the average density vs. the tip-plate distance h for various tip radii R = 10, 20, 30, and 40ℓ (which correspond to 3.7, 7.4, 11.1, and 14.8 nm, respectively). Here, the densities were calculated by averaging the occupancies (0 or 1) of the lattice sites confined between the tip and the plate. The pressure was fixed to 1 atm. Regardless of the tip size, the density was close to 1 when the tip was far away from the plate, but it suddenly dropped to a vapor density <0.5 as h decreased to the threshold value h_c. This dewetting transition occurred at a longer distance h_c as the tip size increased. In other words, the dewetting transition was longer in range for a larger tip.

The plot of h_c vs. the tip radius is shown at the bottom of Fig. 2. The results from the MC simulation (drawn as squares) are compared with the continuum theory (line). For both simulation and theory, h_c increased with the increasing tip radius. This trend is more prominent in the theory. Except for the radius of 10ℓ, the continuum theory significantly overestimated the simulation results.

Next, the effect of pressure on the dewetting transition was investigated. Fig. 3 (top) shows the plot of density vs. h for pressures of 0.08, 1, 8, 25, 50, 75, and 146 atm (the tip radius was fixed to 30ℓ). With increasing pressure, the dewetting transition occurred at a shorter h. It is worth noting that for pressures $\geq$25 atm, the density did not drop to a vapor value (<0.5) with decreasing h. This may be attributed to the fact that the dewetting at such high pressures occurs only locally (near the end of the tip) and not in the entire region below the tip (whereas the density is calculated by averaging over the entire region below the tip). For the two highest pressures, 75 and 146 atm, the dewetting transition was associated with a smooth decrease in the density with decreasing value of h. This smooth change in the density is indicative of supercritical water because of the small cavities formed at these high pressures. At the bottom of Fig. 3, the h_c values from the theory (solid line) and simulation (squares) are plotted vs. pressure.Compared to the simulation results, the theoretical h_c values were overestimated because theoretical cavities are cylindrical whereas the simulated cavities are close to concave menisci (as shown in the bottom of Fig. 4). Using the Young equation, $\Delta\Omega$ in Eq. (1) can be written as $\Delta\Omega = (\Delta P)V + \gamma_{LV}\cos\theta A_{LS} + \gamma_{LV}A_{LV}$. Thus, the $\Delta\Omega$ value of a cylindrical cavity can be compared to that of a meniscus cavity. Assuming that both the cavities have identical values of A_{LS} (identical r values), the sign of $\Delta\Omega$ is determined by the magnitudes of $(\Delta P)V$ and $\gamma_{LV}A_{LV}$, which, respectively, drive (a negative term in $\Delta\Omega$) and hinder (a positive term in $\Delta\Omega$) the dewetting transition. For a typical geometry of the dewetting transition (R = 30l, r/R = 0.4, h = 8l), the V of the cylinder is much larger (by more than twice) than that of the meniscus, while A_{LV} is only slightly greater (by 1.1 times) for the meniscus. Consequently, the $\Delta\Omega$ value in the cylindrical approximation is more negative than that of a meniscus for the same value of h. In other words, the dewetting transition in the cylindrical approximation occurs at a longer distance (h_c). This overestimation of the cavity volume in the cylindrical approximation becomes more significant as the

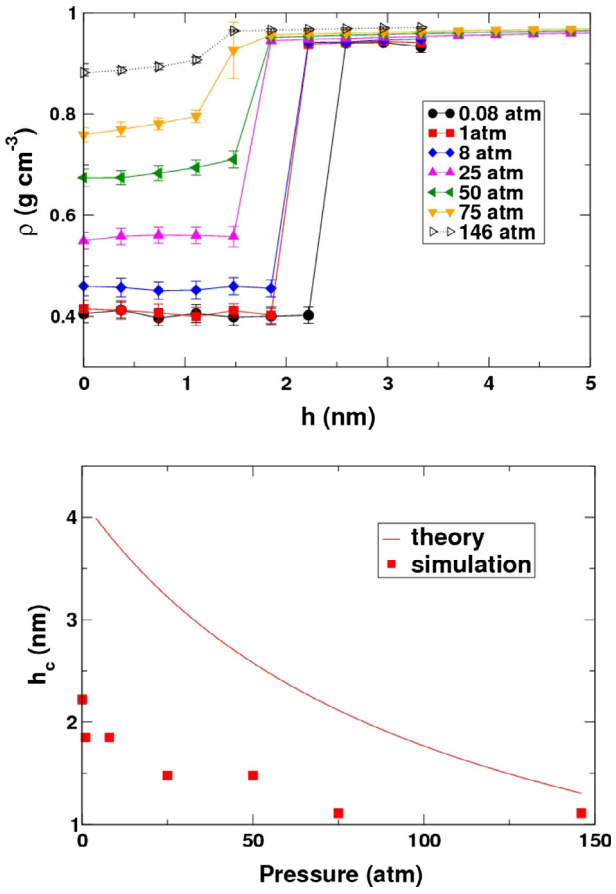

Fig. 3. Effects of pressure on the dewetting transition of water confined between a spherical tip and a plate. Plot of the average density vs. the tip-plate distance h for pressures ranging from 0.08 to 146 atm (top). The error bars represent the standard deviations in the densities. Plot of the tip-plate distance at the dewetting transition h_c vs. pressure (bottom). The theoretical prediction and simulation results are drawn as solid line and squares, respectively.

size of cavity increases. This is consistent with the increased deviation of theory from simulation with decreasing the pressure (Fig. 3, bottom) or the radius of tip (Fig. 2, bottom). Note also that the theory and simulation might differ because of their fundamentally different views of the liquids, i.e., continuum vs. discrete molecule.

The hydrophobic force acting between the tip and the plate was also calculated by varying the tip-plate distance h. The force was attractive (negative) at small h values and it approached zero with increasing h. The magnitude of the maximum attractive force was defined as the *pull-off force* [35]. In the top of Fig. 4, the plot of the pull-off force vs. the tip radius is shown. It is evident from the plot that the pull-off force monotonically increased with the increasing tip radius.

The effect of pressure on the pull-off force was also investigated (Fig. 4, middle). On increasing the pressure from 1 to 146 atm, the pull-off force decreased and then increased. As the cavity shrunk in size with increasing pressure, the force pull-off decreased as the pressure increased from 1 to 50 atm. However, with further increase in pressure, the cavity became smaller and its concave curvature became larger (see the bottom of Fig. 4). Consequently, the Laplace pressure due to the concave curvature increased, resulting in an overall increase in the pull-off force.

Finally, the influence of atomic roughness in the tip and plate surfaces on the dewetting transition was studied. By fixing the tip radius to 20ℓ and the pressure to 1 atm, rectangular bumps with

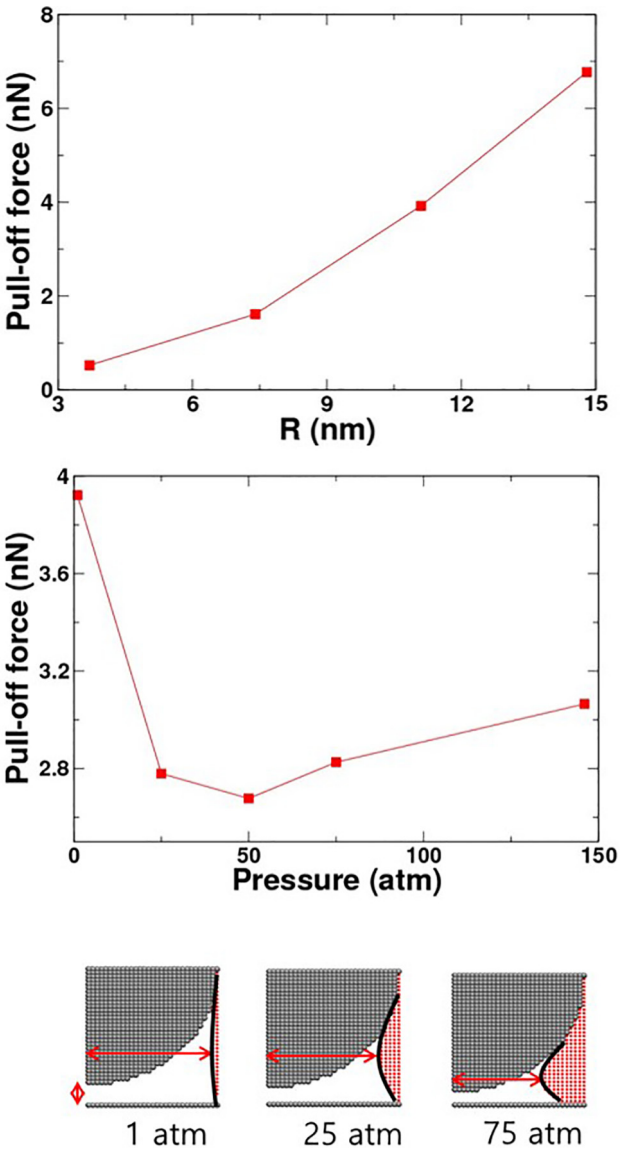

Fig. 4. Hydrophobic force acting between a spherical tip and a plate. The pull-off force vs. the tip radius R (top). Pull-off force vs. pressure (middle). Snapshots of cavities taken at three different pressures (bottom). All the forces are in units of nN. Lines are drawn as a visual guide only.

a width of 3ℓ (1.11 nm) and a height of 2ℓ (0.74 nm) were introduced on both the tip and plate surfaces (Fig. 5, top right). The RMS roughnesses of the tip and plate surfaces were 0.4 nm. With introduction of the surface roughness, the liquid filling the space between the tip and plate (top left of Fig. 5) evaporated. In Fig. 5 (middle), the cavity width is plotted vs. h (drawn as open squares) for the cases with and without the surface roughness. Clearly, the cavity started to form between the rough tip and the plate at a much longer distance ($h = 10\ell$) than that between the smooth tip and plate ($h = 6\ell$). The present theory for the smooth tip and plate predicts a value of $h_c = 5$. It is also noteworthy that the cavities formed between the rough tip and plate were wider than those between the smooth tip and plate.

Fig. 5 (bottom) shows the force-distance curves calculated with and without the surface roughness. The hydrophobic forces for the rough and smooth surfaces were found to be similar to each other for short distances, $h < 6\ell$. With further increase in h, the hydrophobic forces in the two cases diverged. The force between the rough tip and plate (drawn as circles) decayed to zero at h =

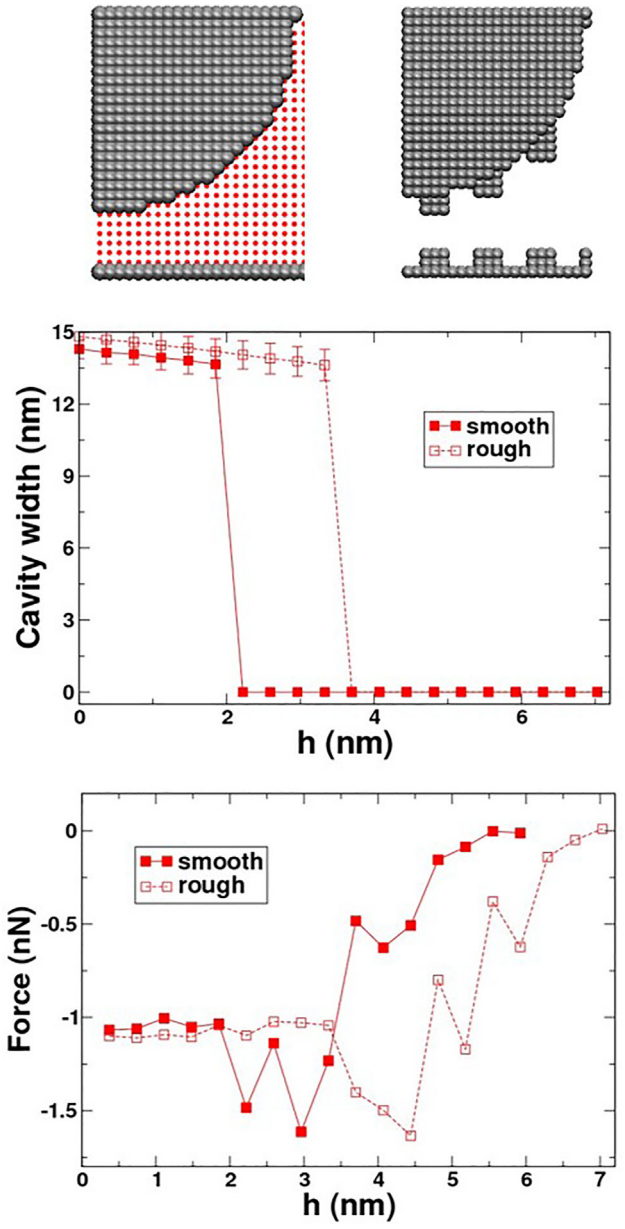

Fig. 5. Dewetting transition of water confined between a rough tip and plate. Simulation snapshots of the tip and plate without (top left) and with (top right) atomic surface roughness. Without the surface roughness, water molecules (drawn as dots) filled the gap between the tip and plate. With the surface roughness, the water molecules evaporated (top right). Cavity width vs. the tip-plate distance h (middle). The results obtained with (open squares) and without (filled squares) the surface roughness have been shown together for comparison. The standard deviations of the cavity widths are drawn as error bars. Hydrophobic force vs. the tip-plate distance h (bottom). The results for the cases with and without roughness are drawn as open and filled squares, respectively. The lines serve as a visual guide only.

19ℓ and was longer in range than the force between the smooth tip and plate (squares), which became zero at $h = 16\ell$. It is worth noting that the forces were non-zero at distances greater than h_c, implying that the hydrophobic force still acts without the presence of a stable cavity (note that only stable cavities with relative fluctuations less than 20% were included in the calculation of the cavity widths). Also, the pull-off force located at $h = 12$ was larger (77.8) than the corresponding value (at $h = 8$) for the smooth tip and plate (76.9).

The present Monte Carlo model previously reproduced the magnitudes and humidity dependencies of the capillary forces measured in atomic force microscopies [24,36]. Therefore, we can use the lattice model to draw qualitative conclusions concerning the dewetting transitions and hydrophobic forces. A quantitative comparison with an experiment seems difficult however, because, besides the inherent limitation of the lattice model, the simulated tips are much smaller than an experimental one and the exact of the geometry of an experimental tip is unknown. The observation that both the dewetting and hydrophobic force were enhanced in range and in magnitude with the atomic surface roughness is consistent with the experiment performed by Singh et al. [15] However, their experiment employed a tip with a diameter of 150 μm (presumably with a microscale surface roughness). A hydrophobic force of a few μNs was measured over the distances of a few μms. On the other hand, the tip simulated in this work was only tens of nms in diameter, while the dewetting was a few nms in range, and the magnitude of the hydrophobic force was a few nNs.

4. Conclusion

The dewetting transition of water confined between a spherical tip and a plate was theoretically studied in the context of atomic force microscopy conducted in water. By utilizing the lattice gas Monte Carlo simulation, we examined the effect of the pressure and the tip-plate distance on the dewetting transition and on the hydrophobic force acting between the tip and the plate. The effect of atomic scale (sub-10 nm scale) roughness in the tip and plate surfaces was also investigated. Even with such small-scale roughness, the dewetting transition was significantly enhanced in range and the hydrophobic force had increased, which is in qualitative agreement with the micrometer scale experiment performed by Singh et al. [15].

Conflict of interest

The authors declare no competing financial interests.

Acknowledgments

This study was supported by the National Research Foundation of Korea (NRF) grant funded by the Korea government (NRF-2015R1A2A2A01004208 and NRF-2014R1A4A1001690).

References

[1] C.M. Dobson, A. Šali, M. Karplus, Protein folding: a perspective from theory and experiment, Angew. Chem. Int. Ed. 37 (7) (1998) 868–893.
[2] C.L. Brooks, M. Gruebele, J.N. Onuchic, P.G. Wolynes, Chemical physics of protein folding, Proc. Natl. Acad. Sci. 95 (19) (1998) 11037–11038.
[3] B. Li, D.O. Alonso, B.J. Bennion, V. Daggett, Hydrophobic hydration is an important source of elasticity in elastin-based biopolymers, J. Am. Chem. Soc. 123 (48) (2001) 11991–11998.
[4] C. Tanford, Hydrophobic free energy, micelle formation and the association of proteins with amphiphiles, J. Mol. Biol. 67 (1) (1972) 59–74.
[5] J.N. Israelachvili, D.J. Mitchell, B.W. Ninham, Theory of self-assembly of hydrocarbon amphiphiles into micelles and bilayers, J. Chem. Soc., Faraday Trans. 2 72 (1976) 1525–1568.
[6] A. Anishkin, S. Sukharev, Water dynamics and dewetting transitions in the small mechanosensitive channel MscS, Biophys. J. 86 (5) (2004) 2883–2895.
[7] R. Roth, D. Gillespie, W. Nonner, R.E. Eisenberg, Bubbles, gating, and anesthetics in ion channels, Biophys. J. 94 (11) (2008) 4282–4298.
[8] F.H. Stillinger, Structure in aqueous solutions of nonpolar solutes from the standpoint of scaled-particle theory, Phys. Chem. Aqueous Syst. (1973) 43–60.
[9] K. Lum, D. Chandler, J.D. Weeks, Hydrophobicity at Small and Large Length Scales, ACS Publications, 1999.
[10] Q.D. Huang, S.W., C.Y. Hua, H.C. Yang, C.L. Chen, J. Chem. Phys. 33 (2004) 745.
[11] X. Huang, R. Zhou, B.J. Berne, Drying and hydrophobic collapse of paraffin plates, J. Phys. Chem. B 109 (2005) 3546–3552.
[12] L. Hua, X. Huang, P. Liu, R. Zhou, B.J. Berne, Nanoscale dewetting transition in protein complex folding, J. Phys. Chem. B 111 (30) (2007) 9069–9077.
[13] P. Liu, X. Huang, R. Zhou, B.J. Berne, Observation of a dewetting transition in the collapse of the melittin tetramer, Nature 437 (7055) (2005) 159.

[14] T. Young, L. Hua, X. Huang, R. Abel, R. Friesner, B. Berne, Dewetting transitions in protein cavities, Proteins: Struct., Funct., Bioinf. 78 (8) (2010) 1856–1869.
[15] S. Singh, J. Houston, F. van Swol, C.J. Brinker, Superhydrophobicity: drying transition of confined water, Nature 442 (7102) (2006) 526.
[16] A. Luzar, K. Leung, Dynamics of capillary evaporation. I. Effect of morphology of hydrophobic surfaces, J. Chem. Phys. 113 (14) (2000) 5836–5844.
[17] K. Leung, A. Luzar, Dynamics of capillary evaporation. II. Free energy barriers, J. Chem. Phys. 113 (14) (2000) 5845–5852.
[18] P.R. ten Wolde, D. Chandler, Drying-induced hydrophobic polymer collapse, Proc. Natl. Acad. Sci. 99 (10) (2002) 6539–6543.
[19] T.F. Miller, E. Vanden-Eijnden, D. Chandler, Solvent coarse-graining and the string method applied to the hydrophobic collapse of a hydrated chain, Proc. Natl. Acad. Sci. 104 (37) (2007) 14559–14564.
[20] J. Dzubiella, Explicit and implicit modeling of nanobubbles in hydrophobic confinement, Anais Acad. Bras. Ciências 82 (1) (2010) 3–12.
[21] A.P. Willard, D. Chandler, The role of solvent fluctuations in hydrophobic assembly, J. Phys. Chem. B 112 (19) (2008) 6187–6192.
[22] H. Kim, S.I. Lee, M.A. Matin, Z. Zhang, J. Jang, M.Y. Ha, J. Jang, Monte Carlo study on the wetting behavior of a surface texturized with domed pillars, J. Phys. Chem. C 118 (45) (2014) 26070–26079.
[23] L. Maibaum, D. Chandler, A coarse-grained model of water confined in a hydrophobic tube, J. Phys. Chem. B 107 (5) (2003) 1189–1193.
[24] J. Jang, G.C. Schatz, M.A. Ratner, Capillary force on a nanoscale tip in dip-pen nanolithography, Phys. Rev. Lett. 90 (15) (2003) 156104.
[25] K. Binder, D. Landau, Capillary condensation in the lattice gas model: a Monte Carlo study, J. Chem. Phys. 96 (2) (1992) 1444–1454.
[26] J. Jang, M. Yang, G. Schatz, Microscopic origin of the humidity dependence of the adhesion force in atomic force microscopy, J. Chem. Phys. 126 (17) (2007) 174705.
[27] J. Jang, M. Ratner, G.C. Schatz, Atomic-scale roughness effect on capillary force in atomic force microscopy, J. Phys. Chem. B 110 (2) (2006) 659–662.
[28] J. Jang, G.C. Schatz, M.A. Ratner, How narrow can a meniscus be?, Phys Rev. Lett. 92 (8) (2004) 085504.
[29] A. Baumgärtner, K. Binder, J.-P. Hansen, M. Kalos, K. Kehr, D. Landau, D. Levesque, H. Müller-Krumbhaar, C. Rebbi, Y. Saito, Applications of the Monte Carlo Method in Statistical Physics, vol. 36, Springer Science & Business Media, 2013.
[30] B.K. Peterson, K.E. Gubbins, Phase transitions in a cylindrical pore: Grand Canonical Monte Carlo, mean field theory and the Kelvin equation, Mol. Phys. 62 (1) (1987) 215–226.
[31] M. Abramowitz, I.A. Stegun, Handbook of Mathematical Functions: With Formulas, Graphs, and Mathematical Tables, vol. 55, Courier Corporation, 1964.
[32] J. Drelich, The significance and magnitude of the line tension in three-phase (solid-liquid-fluid) systems, Colloids Surf., A 116 (1) (1996) 43–54.
[33] J.N. Israelachvili, H. Wennerstroem, Entropic forces between amphiphilic surfaces in liquids, J. Phys. Chem. 96 (2) (1992) 520–531.
[34] K. Lum, A. Luzar, Pathway to surface-induced phase transition of a confined fluid, Phys. Rev. E 56 (6) (1997) R6283.
[35] J. Jang, J. Sung, G.C. Schatz, Influence of surface roughness on the pull-off force in atomic force microscopy, J. Phys. Chem. C 111 (12) (2007) 4648–4654.
[36] J. Jang, G.C. Schatz, M.A. Ratner, Capillary force in atomic force microscopy, J. Chem. Phys. 120 (3) (2004) 1157–1160.